

Experimental results of ground-layer and tomographic wavefront reconstruction from multiple laser guide stars

Michael Lloyd-Hart, Christoph Baranec, N. Mark Milton, Miguel
Snyder, Thomas Stalcup, and J. Roger P. Angel

Center for Astronomical Adaptive Optics, The University of Arizona, Tucson, AZ 85721
mhart@as.arizona.edu

Abstract: We describe results from the first multi-laser wavefront sensing system designed to support tomographic modes of adaptive optics (AO). The system, now operating at the 6.5 m MMT telescope in Arizona, creates five beacons by Rayleigh scattering of laser beams at 532 nm integrated over a range from 20 to 29 km by dynamic refocus of the telescope optics. The return light is analyzed by a Shack-Hartmann sensor that places all five beacons on a single detector, with electronic shuttering to implement the beacon range gate. A separate high-order Shack-Hartmann sensor records simultaneous measurements of wavefronts from a natural star. From open-loop measurements, we find the average beacon wavefront gives a good estimate of ground layer aberration. We present results of full tomographic wavefront analysis, enabled by supplementing the laser data with simultaneous fast image motion measurements from three stars in the field. We describe plans for an early demonstration at the MMT of closed-loop ground layer AO, and later tomographic AO.

© 2006 Optical Society of America

OCIS codes: (010.1080) Adaptive optics; (010.7350) Wavefront sensing; (110.6960) Tomography.

References and links

1. G. A. Tyler, "Merging: a new method for tomography through random media," *J. Opt. Soc. Am. A* **11**, 409–424 (1994).
2. M. Johns, J. R. P. Angel, S. Shectman, R. Bernstein, D. Fabricant, P. McCarthy, and M. Phillips, "Status of the Giant Magellan Telescope (GMT) project," in *Ground-Based Telescopes*, J. M. Oschmann, ed., Proc. SPIE **5489**, 441–453 (2004).
3. L. M. Stepp and S. E. Strom, "The Thirty-Meter Telescope project design and development phase," in *Second Bäckaskog Workshop on Extremely Large Telescopes*, A. L. Ardeberg and T. Andersen, eds., Proc. SPIE **5382**, 67–75 (2004).
4. P. L. Wizinowich et al., "The W. M. Keck Observatory laser guide star adaptive optics system: overview," *Publ. Astron. Soc. Pac.* **118**, 297–309 (2006).
5. A. Tracy, A. Hankla, C. Lopez, D. Sadighi, K. Groff, C. d'Orgeville, M. Sheehan, D. Bamford, S. Sharpe, and D. Cook, "High-power solid-state sodium guidestar laser for the Gemini North Observatory," in *Solid State Lasers XV: Technology and Devices*, H. J. Hoffman and R. K. Shori, eds., Proc. SPIE **6100**, 404–415 (2006).
6. H. Takami et al. "Laser guide star AO project at the Subaru Telescope," in *Advancements in Adaptive Optics*, D. Bonaccini, B. L. Ellerbroek, and R. Ragazzoni, eds., Proc. SPIE **5490**, 837–845 (2004).
7. M. Kasper, J. Charton, B. Delabre, R. Donaldson, E. Fedrigo, G. Hess, N. Hubin, J.-L. Lizon, M. Nylund, C. Soenke, and G. Zins, "LGS implementation for NAOS," in *Advancements in Adaptive Optics*, D. Bonaccini, B. L. Ellerbroek, and R. Ragazzoni, eds., Proc. SPIE **5490**, 1071–1078 (2004).

8. R. Ragazzoni, E. Marchetti, and G. Valente, "Adaptive-optics corrections available for the whole sky," *Nature* **403**, 54–56 (2000).
9. M. Langlois, T. Rimmele, and G. Moretto, "Solar multiconjugate adaptive optics at the Dunn Solar Telescope: preliminary results," in *Advancements in Adaptive Optics*, D. Bonaccini, B. L. Ellerbroek, and R. Ragazzoni, eds., Proc. SPIE **5490**, 59–66 (2004).
10. T. Berkefeld, D. Soltau, and O. von der Lühe, "Second-generation adaptive optics for the 1.5 m solar telescope GREGOR, Tenerife," in *Advancements in Adaptive Optics*, D. Bonaccini, B. L. Ellerbroek, and R. Ragazzoni, eds., Proc. SPIE **5490**, 260–267 (2004).
11. F. Rigaut, "Ground-conjugate wide field adaptive optics for the ELTs," in *Beyond Conventional Adaptive Optics*, E. Vernet, R. Ragazzoni, S. Esposito, and N. Hubin, eds., Vol. 58 of ESO Proceedings Series, (European Southern Observatory, Garching, 2002), pp. 11–16.
12. A. Tokovinin, "Ground layer sensing and compensation," in *Second Bäckaskog Workshop on Extremely Large Telescopes*, A. L. Ardeberg and T. Andersen, eds., Proc. SPIE **5382**, 490–499 (2004).
13. A. Tokovinin, "Seeing improvement with ground-layer adaptive optics," *Publ. Astron. Soc. Pac.* **116**, 941–951 (2004).
14. D. R. Anderson, NRC Herzberg Institute of Astrophysics, 5071 W. Saanich Road, Victoria, BC V9E 2E7, et al., are preparing a manuscript to be called "Modelling a ground layer adaptive optics system".
15. M. Lloyd-Hart, C. Baranec, N. M. Milton, T. Stalcup, M. Snyder, N. Putnam, and J. R. P. Angel, "First tests of wavefront sensing with a constellation of laser guide beacons," *Astrophys. J.* **634**, 679–686 (2005).
16. T. E. Stalcup, J. A. Georges, M. Snyder, C. Baranec, N. Putnam, N. M. Milton, J. R. P. Angel, and M. Lloyd-Hart, "Field tests of wavefront sensing with multiple Rayleigh laser guide stars and dynamic refocus," in *Advancements in Adaptive Optics*, D. Bonaccini, B. L. Ellerbroek, and R. Ragazzoni, eds., Proc. SPIE **5490**, 1021–1032 (2004).
17. R. Q. Fugate, "The Starfire Optical Range 3.5-m adaptive optical telescope," in *Large Ground-Based Telescopes*, J. M. Oschmann and L. M. Stepp, eds., Proc. SPIE **4837**, 934–943 (2003).
18. D. T. Gavel, S. S. Olivier, B. J. Bauman, C. E. Max, and B. A. Macintosh, "Progress with the Lick adaptive optics system," in *Adaptive Optical Systems Technology*, P. L. Wizinowich, ed., Proc. SPIE **4007**, 63–70 (2000).
19. R. Q. Fugate, L. M. Wopat, D. L. Fried, G. A. Ameer, S. L. Browne, P. H. Roberts, G. A. Tyler, B. R. Boeke, and R. E. Ruane, "Measurement of atmospheric wavefront distortion using scattered light from a laser guide-star," *Nature* **353**, 141–146 (1991).
20. J. A. Georges, P. Mallik, T. Stalcup, J. R. P. Angel, and R. Sarlot "Design and testing of a dynamic refocus system for Rayleigh laser beacons," in *Adaptive Optical System Technologies II*, P. L. Wizinowich and D. Bonaccini, eds., Proc. SPIE **4839**, 473–483 (2002).
21. J. Verin, A. Agabi, R. Avila, M. Azouit, R. Conan, F. Martin, E. Masciadri, L. Sanchez, and A. Ziad, "Gemini site testing campaign. Cerro Pachon and Cerro Tololo," Gemini RPT-AO-G0094, <http://www.gemini.edu/> (2000).
22. J. W. Hardy, *Adaptive Optics for Astronomical Telescopes*, (OUP, New York, 1998), Chap. 3.
23. M. Lloyd-Hart and N. M. Milton, "Fundamental limits on isoplanatic correction with multiconjugate adaptive optics," *J. Opt. Soc. Am. A* **20**, 1949–1957 (2003).
24. F. Chassat, *Propagation optique à travers la turbulence atmosphérique. Etude modale de l'anisoplanétisme et application à l'optique adaptative*, PhD thesis, Université Paris-Sud (1992).
25. T. Fusco et al., "NAOS performance characterization and turbulence parameters estimation using closed-loop data," in *Advancements in Adaptive Optics*, D. Bonaccini, B. L. Ellerbroek, and R. Ragazzoni, eds., Proc. SPIE **5490**, 118–129 (2004).
26. B. Le Roux, J.-M. Conan, C. Kulcsár, H.-F. Reynaud, L. M. Mugnier, and T. Fusco, "Optimal control law for classical and multiconjugate adaptive optics," *J. Opt. Soc. Am. A* **21**, 1261–1276 (2004).
27. R. W. Wilson, "SLODAR: measuring optical turbulence altitude with a Shack-Hartmann wavefront sensor," *Mon. Not. R. Astron. Soc.* **337**, 103–108 (2002).

1. Introduction

Key advances in adaptive optics (AO) will be enabled through the deployment of multiple laser guide stars (LGS) [1]. Constellations of beacons may be analyzed to yield a three-dimensional solution to the atmospherically induced wavefront aberration through tomography. Wider compensated fields of view than are now seen with conventional AO systems, even those equipped with single laser beacons, will be achieved with less field dependence of the delivered point-spread function. On telescopes of the current 8–10 m class, multi-conjugate AO (MCAO) using tomographic wavefront sensing is expected to yield correction to the diffraction limit in the near infrared over fields of 1–2 arcmin diameter. Compensation of turbulence close to the ground is anticipated to give substantial improvement over natural seeing for even larger fields up to 10 arcmin.

The promise of these new techniques, which remain almost entirely unexplored at the telescope, is even greater for the next generation of extremely large telescopes (ELTs)[2, 3]. Indeed, the primary motivation for our work at the MMT telescope described here is to understand how to design, build, and operate an AO system for the 25 m Giant Magellan Telescope, where multi-LGS tomographic wavefront sensing will be essential. Because laser beacons are at finite height in the atmosphere, rays of light from LGS sample the atmosphere differently from rays of starlight. The resulting difference between wavefronts measured from a natural star and those from an LGS pointed in the same direction is called focal anisoplanatism. For 8 m telescopes, the error is not so large as to prevent high Strehl imaging in the near infrared with a single LGS, but the error grows with aperture, and for ELTs the error would be prohibitive. It can be overcome however by combining signals from multiple LGS which collectively fill the volume of atmosphere perturbing the starlight.

Current AO systems that rely entirely on natural stars (NGS) for wavefront information are severely restricted to regions of sky with suitably bright guide stars. In contrast, the gains from multi-LGS systems will be realizable over most of the sky, enormously expanding the scientific return from our present and future large telescopes. Indeed, the power of laser systems for science programs is now being demonstrated by the single LGS system on the Keck II telescope [4], with others shortly to come on line [5, 6, 7].

Pioneering work by Ragazzoni et al. [8] has hinted at the power of tomographic wavefront sensing. That paper describes experiments at the Telescopio Nazionale Galileo, in which wavefront estimates were obtained simultaneously from a close asterism of four natural stars through the simple expedient of defocusing the telescope. The instantaneous Zernike modal amplitudes measured from one star were compared to estimates derived from the modal amplitudes of the other three. Tomographic estimation from the three beacon stars was shown to be substantially superior to a simple average, or the use of any one of the three individually.

Of the advanced techniques enabled by tomographic wavefront sensing, only MCAO has yet been attempted, in experiments at two solar telescopes [9, 10]. Numerical models of ground-layer AO (GLAO) based on measurements of the vertical distribution of turbulence at a number of sites [11, 12, 13], suggest the potential for dramatic image improvement in the near infrared. Anderson et al.[14] have modeled GLAO performance in detail, using vertical distributions of turbulence seen at Cerro Pachón that put roughly 2/3 of the power in the ground layer. With a pentagonal arrangement of LGS and an adaptive secondary mirror, the study concluded that the median image width in K band would improve from 0.42 to 0.18 arcsec for a 5 arcmin field and to 0.25 arcsec over 10 arcmin.

In an earlier paper [15], we reported results of open-loop tests of ground-layer wavefront reconstruction using a constellation of five Rayleigh laser guide stars (RLGS) at the MMT. Here, we briefly review the multi-beacon sensing system and the ground-layer results from that paper, and describe further analysis of the data in which the wavefront of a probe star is estimated from a tomographic reconstruction of the RLGS signals and the real-time image motion of other nearby stars. In this case, none of the RLGS nor the tip-tilt stars were coincident with the probe star whose wavefront was to be recovered.

2. Brief description of the beacons and wavefront sensor

For a full description of the laser beacon and tomographic wavefront sensing systems, we refer the reader to previously published accounts [15, 16]. Earlier work on laser-guided AO has been confined to a single beacon, usually created by resonance scattering in the sodium layer at 90 km altitude [4, 17, 18]. For our work at the 6.5 m MMT, we have created five beacons, generated by Rayleigh scattering, with two commercial, pulsed doubled-YAG lasers at 532 nm. Single Rayleigh beacons gated to an altitude of ~ 12 km have previously been used for AO at

small telescopes [19] but the strong focus anisoplanatism and incomplete sampling of higher turbulence make a single such beacon of little value for an 8 m class telescope.

For our experiments, though, Rayleigh beacons are ideal. In our system the range gate is centered at 24 km altitude, high enough to sample collectively most of the turbulence. To increase signal strength, the sensor system includes optics to focus the telescope dynamically, to maintain sharp images of each laser pulse as it rises from 20 to 29 km [16, 20]. In this way, the range gate is extended to be $\sim 20\times$ longer than the telescope's normal depth of field. Even at this high altitude, focus anisoplanatism would remain a difficulty with a single beacon, but with five, it is not an issue, precisely because our goal is the development of tomographic techniques.

The five beacons, each with a projected power of 4 W, are arranged in a regular pentagon of 2 arcmin diameter. The return flux at zenith has been measured at 1.1×10^5 photoelectrons $\text{m}^{-2}\text{J}^{-1}$ over the full range gate. The images from all five beacons are recorded on a novel implementation of the Shack-Hartmann wavefront sensor (WFS), which includes the dynamic focus optics and a single electronically shuttered CCD. A prism array at the exit pupil divides it into 60 subapertures of equal area arranged in a hexapolar geometry.

A separate conventional Shack-Hartmann sensor looking at a natural star provides simultaneous ground-truth wavefront information for comparison with reconstructions from the LGS. The NGS sensor can be moved in order to probe different regions within the LGS constellation. In addition, a fast-framing camera with 2.5 arcmin field of view images the field in and around the LGS constellation. By tracking a suitable asterism, rapid tip-tilt signals from natural stars in this field are recorded as an aid to the tomographic reconstruction.

3. Data analysis

For the open-loop results described here, the three wavefront sensing cameras were run at typical rates of 50 and 100 fps. A typical data set comprises continuous 60-s sequences of frames from all three cameras simultaneously. Wavefronts are reconstructed on the Zernike basis set from the NGS and each of the five LGS separately, and the image motions from stars in the wide-field camera are estimated by a correlation tracking algorithm with a gaussian template. Figure 1 illustrates the output from the three cameras and the reconstructed wavefronts derived from them.

3.1. Summary of GLAO results

The ground layer contribution to stellar wavefront aberration is computed as the average of the wavefronts reconstructed from the individual LGS beacons. Atmospheric turbulence close to the ground is common to the star and each LGS beacon, while higher altitude aberration, different for each beacon, will be mitigated in the average. Since all field points share this common ground layer turbulence, the use of GLAO promises a reduction of stellar wavefront aberration over a wide field. The technique is likely to be valuable because it is found empirically that up to two thirds of atmospheric turbulence is typically located near the ground [21].

Wavefront recoveries using this approach, under seeing conditions of ~ 1.1 arcsec, are described in detail in our earlier paper [15]. Since then, we obtained additional data in seeing of ~ 0.5 arcsec ($r_0 = 22$ cm at 500 nm wavelength), at the 15th percentile for the site measured over the past two years. In both cases, the fidelity of the estimation across the field encompassed by the LGS was investigated by offsetting the telescope and the beacons with respect to the NGS. The ground layer wavefront reconstruction estimated the 25 modes of Zernike orders 2 through 6 from the LGS. Figure 2 shows the residual stellar wavefront error after GLAO correction as a function of angle from the center of the LGS constellation. Ground layer correction of the data taken in poorer seeing yielded an average 38% improvement in RMS wavefront aberration over the full field enclosed by the beacons, and extended well outside the constellation. For the new

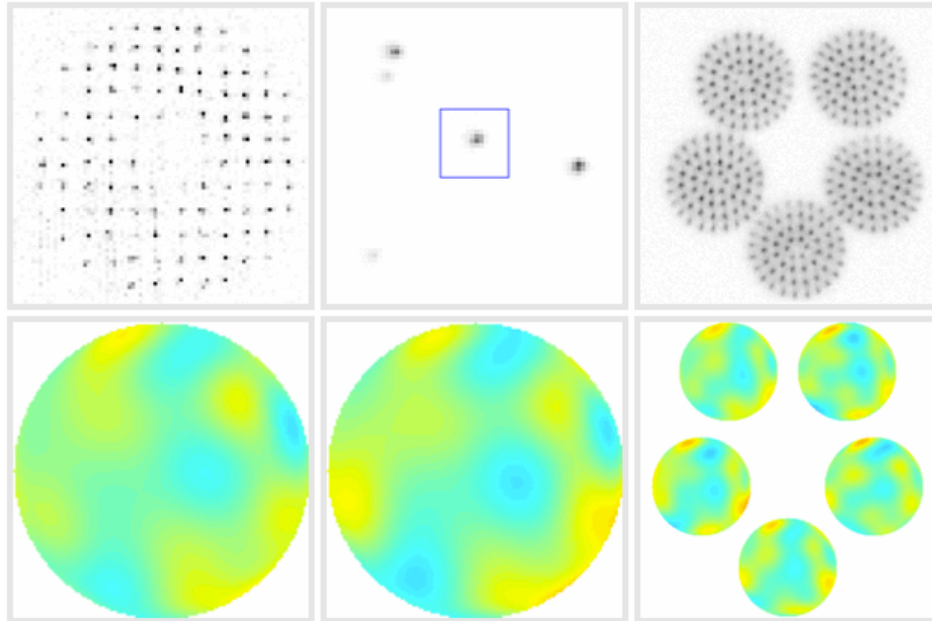


Fig. 1. Sample data from the three real-time cameras and the corresponding reconstructed wavefronts. The movie (1.8 MB) shows on the top row, from left to right, continuous and simultaneous sequences of frames from the NGS Shack-Hartmann sensor, the wide field asterism camera, and the LGS Shack-Hartmann sensor. (The star images in the asterism have been magnified $\times 4$ compared to their spacing.) The boxed star in the asterism is the same as used on the NGS sensor; the light is split between the two. The lower panels show the reconstructed NGS wavefront (left), the individual LGS wavefronts (right) and the NGS wavefront as estimated by tomography (center).

data, when the seeing was already excellent, ground layer correction was consistently beneficial across the field, although the fractional improvement within the constellation was actually less at 25%, with correction not extending as far beyond the beacon radius. Across this broad range of conditions, spanning roughly the middle half of the probability density function of seeing at the MMT, the point-spread function (PSF) delivered by a closed-loop system would show morphological variation much less than one would expect from the raw seeing. Furthermore, this result suggests that ground-layer correction with LGS will be a powerful tool for recovering good image quality especially when the native seeing is worse than median.

A key parameter for GLAO is the thickness of the boundary layer, since it determines the corrected field of view. Very little is known about the boundary layer from current site surveys because the GLAO concept is quite recent, and the ground layer thickness has almost no impact on any other observing mode of a telescope. We have estimated the thickness during our observations by a method described in [15] which examines the anisoplanatic behavior of the stellar wavefront with respect to the individual LGS wavefronts. The RMS difference between the two with angular separation θ is expected to grow as $(\theta/\theta_0)^{5/3}$. The isoplanatic angle θ_0 for the ground layer is related to the turbulence-weighted mean height h of the layer through $\theta_0 = 0.314 \cos \zeta r_0/h$ [22]. For the observations of September 2004, we find $h = 380$ m. For the June 2005 data, despite the lower absolute strength of the ground layer, its mean height was greater, with $h = 530$ m.

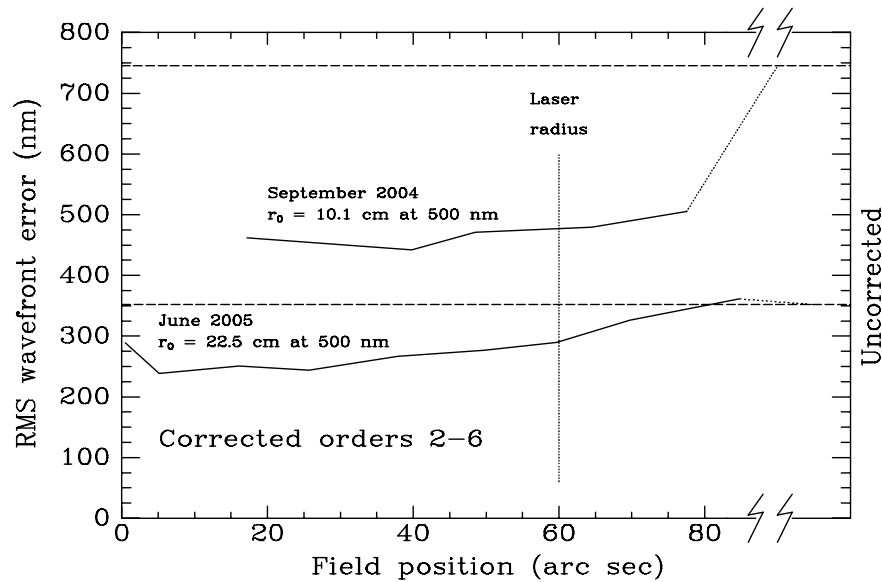


Fig. 2. Wavefront correction of starlight on the basis of the average LGS signals. The dashed lines show the uncorrected error while the solid lines show the RMS residual wavefront phase after ground layer correction as a function of angular distance between the star and the geometric center of the LGS constellation. Tilt (global image motion) is excluded since it is not sensed by the lasers.

3.2. Tomographic reconstruction along a single line of sight

The tomographic solution of the beacon wavefronts in principle yields a three-dimensional view of the aberration. In the simplest application, the instantaneous wavefront from an astronomical object is estimated by integration through the volume along the line of sight to the object, and the compensating phase is applied to a single deformable mirror (DM). The technique, called laser tomography AO (LTAO), delivers a diffraction-limited field of view limited by the normal isoplanatic angle. Each of the steps of this process, illustrated in Fig. 3, is linear. In practice therefore, all the steps may be multiplied to give a single linear function. In this way, LTAO can be implemented in a conventional way through a matrix multiplication of the combined vector of slopes from all the beacons to yield a command update to the DM. For clarity in our analysis, we have chosen first to reconstruct separately the wavefronts from each of the LGS and then to apply a tomographic reconstructor matrix to estimate the wavefront of the probe star.

Data from the three real-time cameras have been analyzed in this way. Spot positions in the Shack-Hartmann patterns recorded on the LGS WFS were extracted frame by frame to a precision of 0.03 pixels (0.026 arcsec) by finding the local peaks in the correlation of the data with a gaussian of width 1.8 pixels. For each 60 s data set, the mean position of each spot was subtracted from its instantaneous position, thereby removing the effects of telescope aberration and long-term collimation drift. Wavefronts from each LGS were then reconstructed from the residual spot positions by fitting the first 44 Zernike modes (orders 1 through 8) using a synthetic reconstructor matrix derived from a model of the prism array in the WFS optics.

In a closed-loop system, the reconstructed LGS tilt modes would be used to control beam jitter by driving a fast steering mirror in the laser beam projector optics, but for this open-loop analysis they are discarded. Instead, the higher order LGS measurements are supplemented by the image motion from three stars in the wide field asterism camera, shown in Fig. 4. The

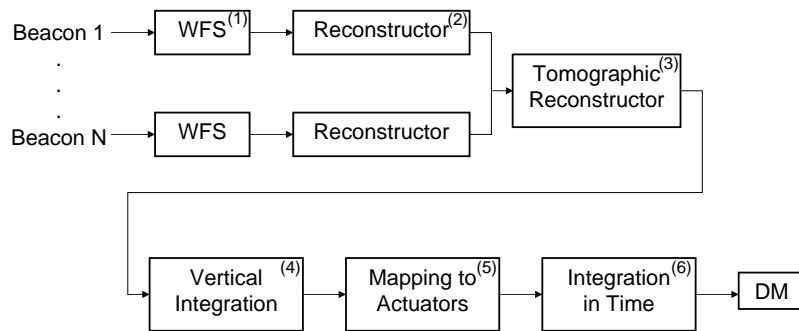


Fig. 3. The processing sequence for laser tomography AO. Light from each beacon is recorded by a wavefront sensor (1), and the individual beacon wavefronts are reconstructed (2). The three-dimensional structure of the aberration is recovered by tomography (3). A spatial integration along the line of sight estimates the stellar aberration (4), which is mapped onto the DM actuators (5) and (in a closed-loop AO system) integrated in time to give the required actuator commands (6). In practice, steps (2) through (5) can be implemented as a single matrix-vector multiplication.

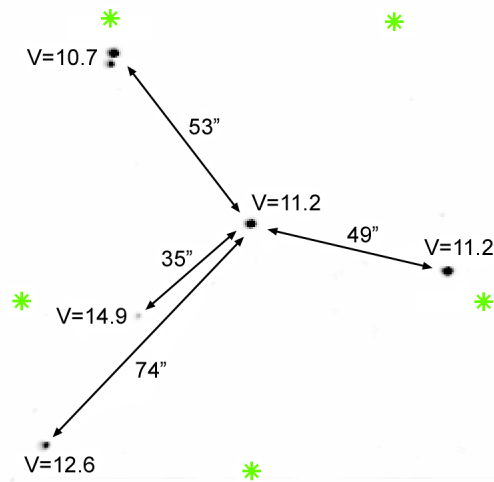


Fig. 4. Sample frame from the asterism camera. Light from the central star was also fed to the NGS WFS. Image motion of the three brightest stars surrounding this one were used to estimate global tilt and second order modes in the tomographic reconstruction. The positions of the beacons are illustrated by the green stars. To account for field rotation, the LGS pattern was rotated in the beam projector optics, maintaining a fixed orientation with respect to the asterism as the MMT tracked.

stars allow determination of the tilt terms in the central probe star's wavefront, and a three-dimensional solution to the second-order terms focus and astigmatism [23]. Separately, the wavefronts from the probe star were reconstructed to the same order from the NGS sensor measurements. For comparison, a ground layer estimate of the probe star's wavefront was also reconstructed from these data.

Our tomographic reconstruction assumes a linear relation between the wavefront of the probe star and those of the LGS, represented by the equation

$$\hat{\mathbf{a}}_{ps} = \mathbf{T}\mathbf{b} \quad (1)$$

where $\hat{\mathbf{a}}_{ps}$ is the vector of Zernike polynomial coefficients characterizing the estimate of the probe star wavefront, \mathbf{b} is a vector containing the Zernike coefficients of all the reconstructed LGS wavefronts and the tilt measurements from the three field stars, and \mathbf{T} is the tomographic reconstructor matrix relating the two. We wish to find a tomograph \mathbf{T} that minimizes $\langle |\mathbf{a}_{ps} - \hat{\mathbf{a}}_{ps}|^2 \rangle$, the squared norm of the difference between the measured probe star wavefront coefficients \mathbf{a}_{ps} and their estimates, averaged over time. The coefficients are scaled so that this also minimizes the RMS residual phase in the reconstructed wavefront.

To investigate the limit of tomographic performance permitted by the data in this least squares sense, we have derived \mathbf{T} by a direct inversion of the data, using singular value decomposition (SVD). This approach does not rely on any *a priori* model of the atmospheric C_n^2 profile or knowledge of the noise characteristics. A matrix \mathbf{B} is constructed from 3057 data vectors \mathbf{b} , and inverted with SVD to give \mathbf{B}^\dagger . A similar matrix \mathbf{A}_{ps} is constructed from the corresponding \mathbf{a}_{ps} vectors. The tomograph is then given by

$$\mathbf{T} = \mathbf{A}_{ps}\mathbf{B}^\dagger. \quad (2)$$

Applying \mathbf{T} to vectors \mathbf{b} drawn from the same data set used to compute it yields the best fit solution and characterizes the noise floor in the data.

The noise sources fall into two broad categories. The first comprises instrumental effects such as read noise and charge diffusion in the WFS, and photon noise from the lasers. These can be reduced by better (and generally more expensive) hardware. The second arises because of atmospheric effects: broadening of the LGS images by turbulence in the uplink, speckle structure in the NGS Shack-Hartmann sensor spots, and aliasing of high altitude aberrations that are not well sensed by the chosen LGS constellation. These are more difficult to overcome. A full discussion of these in the context of the MMT experiments is beyond the scope of this paper, and will be addressed in a later publication.

We find, as expected, that our tomographic approach yields a substantially better estimate of the probe star's wavefront than the corresponding ground layer recovery. To illustrate, Fig. 5 shows the evolution of the focus term in the probe star's wavefront over a 10 s period and its GLAO and LTAO estimates. Figure 6a shows the RMS wavefront error averaged over the full

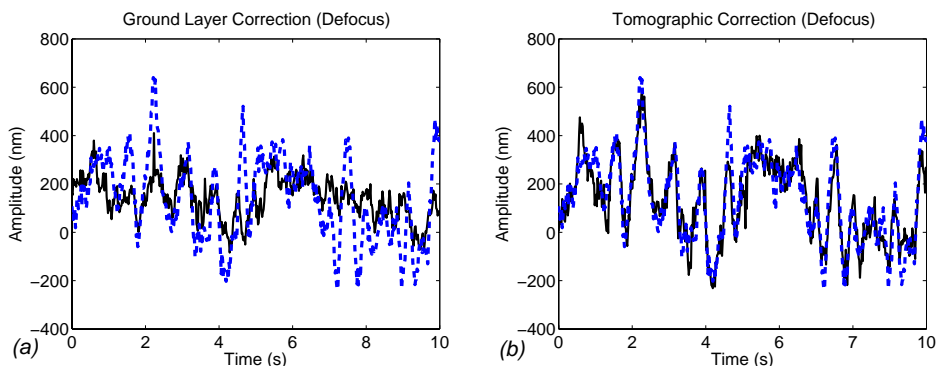


Fig. 5. Evolution of focus in the probe star's wavefront, shown in blue on the two plots, with the ground layer estimate (a) and tomographic estimate (b) plotted in black.

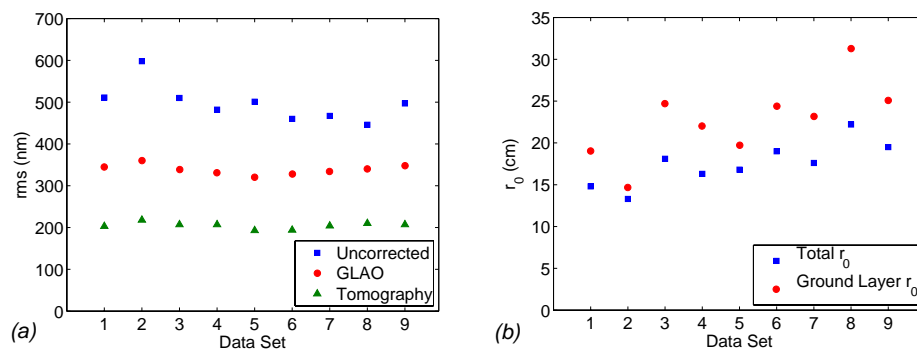


Fig. 6. For each of 9 data sets, each 60 s long, (a) shows the RMS wavefront error summed over orders 2–8 for the probe star wavefront without correction (blue squares), and with GLAO (red circles) and LTAO (green triangles) correction. Values of r_0 , shown in (b) for a wavelength of 500 nm at zenith, have been computed for the total seeing (blue squares) and the ground layer contribution (red circles) only. The data sets were recorded over a 2 hour period and are here numbered chronologically.

60 s of each of 9 data sets, recorded over a period of 2 hours. The values reflect the contributions from the modes through order 8 that were reconstructed, with the exception of tip and tilt. These two modes contain the majority of the wavefront error, but are not sensed by the lasers and therefore give a somewhat misleading sense of the overall degree of correction.

Values of r_0 for each data set are shown in Fig. 6b at a wavelength of 500 nm and corrected to zenith. We start by computing values for the mean square aberration in the modes of each Zernike radial order separately. Applying the formalism developed by Chassat [24] then yields estimates of both r_0 and the outer scale of turbulence L_0 . Our estimates of L_0 range from 12 m to 25 m over the 2 hour period during which the data were recorded, in line with other observations at good sites [25]. (We note in passing that the variable directly estimated by Chassat's method is D/L_0 , where D is the telescope diameter. The truncated forms of the infinite sums given in Refs. 24 and 25, appropriate for the small apertures used in those studies, must be extended in our case where $D/L_0 > 0.25$.) Also shown in Fig. 6b are values for the ground layer turbulence, computed in the same manner from the strength of the Zernike modes of the ground layer estimate from the LGS. We find the average distribution of turbulence for these data puts 70% of the power in the boundary layer with the remainder at higher altitude. This represents an upper limit, since high altitude aberration on large spatial scales will remain partially correlated in the LGS signals and be indistinguishable from true ground layer aberration.

The plots of Fig. 6 show a consistent improvement with both types of wavefront compensation. Of particular note is data set 2, which stands out from its neighbors as having distinctly worse seeing. Yet after ground layer correction, the residual aberration is reduced almost to the same level in all three cases, indicating that the momentary worsening was attributable to a low lying phenomenon.

3.3. Synthetic point-spread functions

From the residual wavefront errors after either ground layer or tomographic estimation at each time step, a synthetic corrected PSF can be calculated. Figure 7 shows examples computed for a source on axis in K band ($2.2 \mu\text{m}$) from a 60 s continuous data sequence recorded in seeing conditions of $r_0 = 14.7 \text{ cm}$ at 500 nm wavelength. The reconstruction estimated the first 44 modes of the probe star's wavefront, now including tip-tilt. To generate realistic instantaneous PSFs

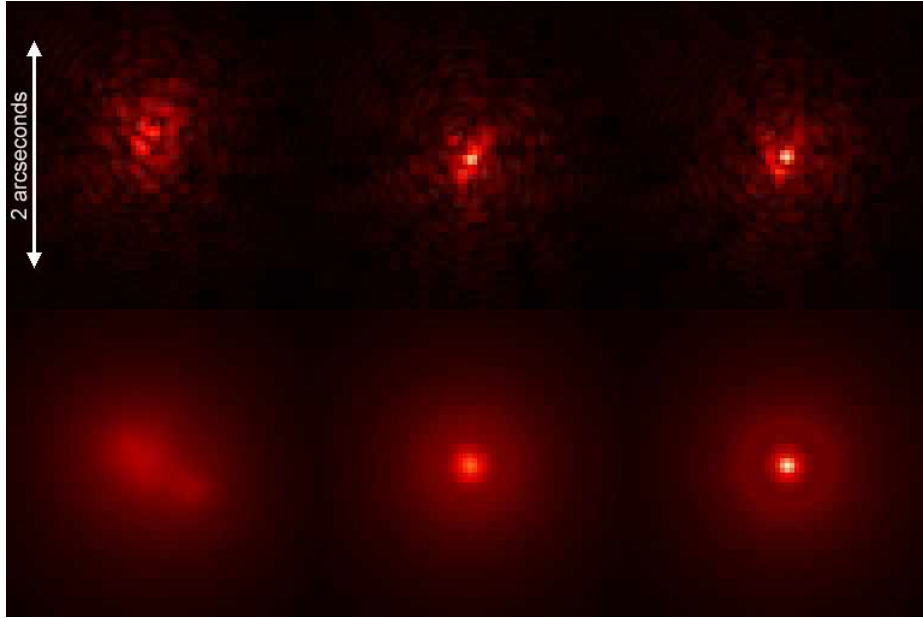


Fig. 7. Synthetic point-spread functions computed at $2.2 \mu\text{m}$ wavelength from wavefronts before and after correction. The movie (1 MB) shows PSFs with no correction (left), with GLAO correction (center), and with LTAO correction (right) over a 10 s period. The frame rate has been slowed from the original 50 Hz to 15 Hz. The lower panels show PSFs averaged over the full 60 s sequence.

for the movie of Fig. 7, the wavefronts were augmented with temporally correlated Zernike modes from orders 9 through 30 drawn from an uncompensated Kolmogorov distribution. The integrated PSFs in Fig. 7 include uncompensated Zernike modes from orders 9 through 100.

Table 1 below shows the corresponding widths and relative peak intensities for the time averaged PSFs, and for PSFs computed similarly in the J band ($1.25 \mu\text{m}$) and H band ($1.65 \mu\text{m}$). Ground layer correction is of particular value in the two longer wavebands, where the image width is reduced by a factor of ~ 4 , and there is a substantial increase in peak intensity. Given that the seeing at the time the data were taken was at about the 50th percentile for the telescope, one can expect closed-loop GLAO performance at ~ 0.2 arcsec or better in H and K bands for the majority of the time.

Table 1. Image quality metrics at $1.25 \mu\text{m}$, $1.65 \mu\text{m}$ and $2.2 \mu\text{m}$.

Metric	Waveband	Uncorrected	GLAO	LTAO	Diffraction limit
FWHM (arcsec)	J	0.771	0.384	0.100	0.040
	H	0.651	0.162	0.081	0.052
	K	0.543	0.123	0.088	0.070
Relative peak intensity	J	1.0	2.0	4.1	485
	H	1.0	3.3	8.3	212
	K	1.0	6.0	13.5	82.5

With tomographic correction, the K band is corrected almost to the diffraction limit, with a 14-fold increase in peak intensity to a Strehl ratio of 16%. The relatively low order reconstruction is insufficient to achieve the diffraction limit at the shorter wavelengths, but the improvement in resolution and peak brightness are both substantial.

4. Conclusion

We have taken the first steps in exploring the practical techniques required for tomographic wavefront sensing. With 60 subapertures placed over the MMT's 6.5 m aperture and with the WFS running at 100 Hz, both the spatial and temporal scales of the wavefront estimation were modest. Nevertheless, we can now say with confidence that there are no fundamental obstacles to closed-loop AO systems with multiple LGS driving altitude conjugated correction.

Our own work at the MMT will see the implementation of both GLAO and LTAO with the MMT's adaptive secondary mirror. Both techniques will benefit from extensions of the reconstructors used for the open loop results to date. The former will likely be improved by a tomographic analysis to identify the ground layer contribution with greater fidelity than the simple average of the LGS wavefronts. This would render more uniform PSFs within the corrected field. Tomographic recovery in general will show improved accuracy and robustness by the incorporation of *a priori* statistical knowledge of the atmospheric aberration and the system noise and optimal linear filtering [26]. The application of these principles, well studied theoretically, to our tomographic data is a high priority for future work.

A new LGS wavefront sensor instrument package, designed as a tool for scientific production has now been completed; in April 2006 it was successfully checked out in a 5-night run at the MMT with the adaptive secondary in open loop. Early application to scientific programs will focus on seeing improvement with GLAO, taking advantage of existing near infrared instrumentation. This choice is motivated by a number of considerations. Not only is GLAO the easiest multi-beacon technique to implement, but the MMT's system is likely to remain unique for several years. The exploitation of routine near infrared seeing of 0.2 arcsec or better over a field of several arcminutes is likely to be very productive, both for imaging and high resolution multi-object spectroscopy where the many-fold improvement in encircled energy within 0.2 arcsec will be of particular value.

Further exploration of tomography will investigate the components of the algorithm outlined in Fig. 3. We will start with the recovery of C_n^2 profiles from two sets of open-loop LGS data, taken close together in time, where the probe star is first on axis and then further out in the field of the LGS constellation. The technique to determine the profiles is very similar to slope detection and ranging (SLODAR) [27]. The derived profiles will be collapsed into a small number of layers. A tomographic reconstructor matrix will be computed to solve for the instantaneous shapes of DMs taken to be at each of these layers. The tomograph will be applied to the NGS data in the two cases, to explore the fidelity and field dependence of MCAO correction.

Closed-loop LTAO, relying just on the adaptive secondary, will be tested in parallel with GLAO. The hardware required is identical for each, with only the elements of the reconstructor matrix to be changed. This suggests a new avenue for research, in which the corrected field of view and the degree of wavefront compensation are traded against each other according to the demands of the immediate science program and the prevailing atmospheric conditions. The MMT system will be uniquely placed to explore this parameter space.

Acknowledgements

This work has been supported by the Air Force Office of Scientific Research under grant F49620-01-1-0383 and the National Science Foundation under grant AST-0138347. Observations reported here were made at the MMT, a joint facility of the University of Arizona and the Smithsonian Institution. We are grateful for the continued support of the MMT Observatory staff, particularly M. Alegria, A. Milone, and J. McAfee. We thank the referee who alerted us to the work of F. Chassat.